Stratum is required for both apical and basolateral transport through stable expression of Rab10 and Rab35 in *Drosophila* photoreceptors

Yuka Ochi†, Hitomi Yamashita†, Yumi Yamada, Takunori Satoh, and Akiko K. Satoh*
Program of Life and Environmental Science, Graduate School of Integral Science for Life, Hiroshima University, 1-7-1 Kagamiyama, Higashi-Hiroshima, Hiroshima 739-8521, Japan

ABSTRACT **Post-Golgi transport for specific membrane domains, also termed polarized transport, is essential for the construction and maintenance of polarized cells. Highly polarized *Drosophila* photoreceptors serve as a good model system for studying the mechanisms underlying polarized transport. The Mss4 *Drosophila* ortholog, Stratum (Strat), controls basal restriction of basement membrane proteins in follicle cells, and Rab8 acts downstream of Strat. We investigated the function of Strat in fly photoreceptors and found that polarized transport in both the basolateral and the rhabdomere membrane domains was inhibited in *Strat*-deficient photoreceptors. We also observed 79 and 55% reductions in Rab10 and Rab35 levels, respectively, but no reduction in Rab11 levels in whole-eye homozygous clones of $Strat^{null}$. Moreover, Rab35 was localized in the rhabdomere, and loss of Rab35 resulted in impaired Rh1 transport to the rhabdomere. These results indicate that Strat is essential for the stable expression of Rab10 and Rab35, which regulate basolateral and rhabdomere transport, respectively, in fly photoreceptors.**

Monitoring Editor
Patrick Brennwald
University of North Carolina, Chapel Hill

Received: Dec 3, 2021
Revised: Jun 21, 2022
Accepted: Jun 23, 2022

INTRODUCTION

Post-Golgi transport for specific membrane domains, also called polarized transport, is essential for the development and maintenance of polarized cells (Román-Fernández and Bryant, 2016). The *Drosophila* retina is an excellent model system for studying the mechanism of polarized transport. In a single cross-section of the *Drosophila* retina, three types of plasma membrane domains (a rhabdomere, stalk, and basolateral membrane) of many photoreceptors are simultaneously observed. Rh1, the rhodopsin expressed in R1–6 outer retinal photoreceptor cells, is specifically localized to an apical membrane domain, the rhabdomere. In contrast, the sodium-potassium ATPase (Na^+/K^+-ATPase) is localized to the basolateral membrane domain.

The Rab family of small GTP-binding proteins is an important regulator of membrane trafficking. More than 60 mammalian and 31 *Drosophila* Rab proteins regulate specific transport steps and pathways (Stenmark, 2009; Pfeffer, 2013). In *Drosophila* photoreceptors, Rab11 regulates the post-Golgi transport of Rh1 to the rhabdomere, and Rab10 is required for the post-Golgi transport of Na^+/K^+-ATPase to the basolateral membrane domain (Satoh *et al.*, 2005; Nakamura *et al.*, 2020). However, other Rab proteins might be involved in post-Golgi transport in fly photoreceptors. The function of Mss4 has been controversial for a long time. Mss4 and its *Saccharomyces cerevisiae* ortholog Dss4 were originally isolated as the first putative Rab guanine nucleotide exchange factor (GEF) (Burton *et al.*, 1993; Moya *et al.*, 1993). Several studies have demonstrated the GEF activity of Mss4 in vitro (Burton *et al.*, 1993; Moya *et al.*, 1993; Burton *et al.*, 1994; Miyazaki *et al.*, 1994; Coppola *et al.*, 2002); however, some studies have indicated that the GEF activity of Mss4 is rather

This article was published online ahead of print in MBoC in Press (http://www.molbiolcell.org/cgi/doi/10.1091/mbc.E21-12-0596) on June 29, 2022.

†These authors contributed equally to this work.

Author contributions: conceptualization, A.K.S.; investigation, Y.O., H.Y., and Y.Y.; writing—original draft, T.S. and A.K.S.; supervision, T.S. and A.K.S.; project administration, A.K.S.; funding acquisition, A.K.S. and T.S.

Competing interests: All authors have read and approved this work and declare that they have no financial conflicts of interest.

*Address correspondence to: Akiko K. Satoh (aksatoh@hiroshima-u.ac.jp).

Abbreviations used: AJs, adherence junctions; GEF, guanine nucleotide exchange factor; IRS, interrhabdomeric space; Strat, Stratum; TGN, *trans*-Golgi network.

weak compared with that of other typical GEFs (Itzen *et al.*, 2006; Itzen *et al.*, 2007). Given its tight binding to nucleotide-free Rabs, Mss4 has been proposed to function as a nucleotide-free chaperone (Nuoffer *et al.*, 1997; Strick *et al.*, 2002; Wu *et al.*, 2014). In agreement with this notion, Mss4 was shown to promote the stability of Rab10 against proteasome degradation and to play crucial roles in glucose transporter type 4 (GLUT4) exocytosis in vivo (Gulbranson *et al.*, 2017). In *Drosophila*, the Mss4 ortholog Stratum (Strat) controls the basal restriction of basement membrane proteins in follicle cells, and Rab8 acts downstream of Strat (Devergne *et al.*, 2017). Strat is also known to localize Rab8 in the *trans*-Golgi network (TGN) and regulate the exit of Notch, Delta, and Spdo from the TGN. Furthermore, it is involved in the stable expression of Rab8 and Rab10 but not Rab1, Rab11, and Rab3 (Bellec *et al.*, 2018; Bellec *et al.*, 2020). Strat was also shown to interact with Rab3, Rab10, and Rab35 in a genomewide interaction map (Guruharsha *et al.*, 2011). In this study, we investigated the impact of Strat deficiency on polarized transport in fly photoreceptors and found that Strat is required for both rhabdomere and basolateral transport through stable expression of Rab10 and Rab35.

RESULTS

Strat is required for both rhabdomere and basolateral transport

R1–6 outer retinal photoreceptor cells contain three different plasma membrane domains: rhabdomere, stalk, and basolateral membranes (Supplemental Figure S1). The rhabdomere is a tight bundle of photoreceptive microvilli protruding from the photoreceptor into the central lumen of the ommatidium. The rhabdomeres appeared oval in the cross-sections of the photoreceptors. Rh1 is an excellent marker of rhabdomere membranes. The basolateral membrane is a Na^+/K^+-ATPase-positive membrane that contacts pigment cells and neighboring photoreceptors. The stalk membrane, positive for Crb, is located between the rhabdomere and the basolateral membrane and faces the interrhabdomeric space (IRS) (Tepass and Harris, 2007; Xiong and Bellen, 2013; Schopf and Huber, 2017; Laffafian and Tepass, 2019).

To understand whether Strat is necessary for post-Golgi transport in these three plasma membranes, we investigated the homozygous photoreceptor phenotypes of the $Strat^{null}$ and $Strat^{WT}$ alleles (Bellec *et al.*, 2018) using a mosaic retina formed by the FLP/FRT method (Xu and Rubin, 1993). The P3RFP markers in the original $Strat^{null}$ and $Strat^{WT}$ alleles were removed using Cre recombinase to visualize heterozygous and wild-type RFP-positive and homozygous *Strat* alleles as RFP-negative in FLP/FRT mosaic retinas. In $Strat^{null}$ homozygous photoreceptors, Na^+/K^+-ATPase was mislocalized in the stalk membrane (Figure 1A, top panel). Together with the shrinkage of the basolateral membrane and the expansion of the stalk membrane, these phenotypes were similar to those of *Rab10*-deficient photoreceptors (Figure 1B). At the same time, $Strat^{null}$ homozygous photoreceptors accumulated Rh1 in the cytoplasm (Figure 1A, top panel) which resembles that in Rab11-reduction by Rab11RNAi^{pWIS}-expression (Figure 1C). In contrast, in $Strat^{WT}$ homozygous photoreceptors (Figure 1A, bottom panel), Na^+/K^+-ATPase and Rh1 localized normally in the basolateral and rhabdomere domains. We also investigated the phenotypes of the Strat RNAi-expressing photoreceptors (Figure 1D). Similar to $Strat^{null}$ homozygous photoreceptors, Strat RNAi^{GD10605}-expressing photoreceptors accumulated Rh1 in the cytoplasm, Na^+/K^+-ATPase was mislocalized to the stalk membrane, and shrinkage of the basolateral membrane and expansion of the stalk membrane were observed in these cells. The stalk and basolateral membranes in $Strat^{null}$ homozygous photoreceptors were longer (1.44×) and shorter (0.56×) than those of the wild-type photoreceptors, respectively, in the same cross-section of the mosaic retina (Figure 1E). The stalk and basolateral membranes in Strat RNAi^{GD10605}-expressing photoreceptors were also longer (1.42×) and shorter (0.70×), respectively, than those of the wild-type photoreceptors in the same cross-section of mosaic retinas (Figure 1E). Quantification of the ratio of Rh1 staining in the cytoplasm against that in the whole photoreceptor that includes both rhabdomeres and cytoplasm confirmed 74 and 81% Rh1 staining in the cytoplasm of $Strat^{null}$ homozygous and Strat RNAi^{GD10605}-expressing photoreceptors, respectively (Figure 1F).

To perform a detailed phenotypic comparison of the wild-type, $Rab10^{null}$, Rab11RNAi, and *Strat*-deficient photoreceptors, we observed thin sections of pupal photoreceptors using electron microscopy (Figure 2, A–J, and Supplemental Figure S2, A–J). In agreement with the data obtained by confocal microscopy, we found that the basolateral and stalk membranes of $Strat^{null}$ homozygous photoreceptors appeared shorter and longer than those of the wild-type photoreceptors, respectively (Figure 2, A and D, and Supplemental Figure S2, A and D), similar to those of $Rab10^{null}$ homozygous photoreceptors (Figure 2B and Supplemental Figure S2B). The basolateral and stalk membrane lengths of the wild-type photoreceptors were 12.49 ± 0.40 µm and 5.28 ± 0.08 µm, respectively (Figure 2K). In contrast, the basolateral and stalk membrane lengths of $Strat^{null}$ homozygous photoreceptors were 8.63 ± 0.76 µm and 6.29 ± 0.50 µm, and those of Strat RNAi^{GD10605}-expressing photoreceptors were 8.47 ± 0.55 µm and 7.15 ± 1.76 µm, respectively (Figure 2K). Thus in $Strat^{null}$ homozygous photoreceptors and Strat RNAi^{GD10605}-expressing photoreceptors, the cross-sectional lengths of the basolateral membranes were 0.69× and 0.68× shorter and those of stalk membranes were 1.19× and 1.35× longer than those of the wild-type photoreceptors, respectively; however, the difference between the stalk membranes lengths of the wild-type and Strat RNAi^{GD10605}-expressing photoreceptors was not significant. In the case of $Rab10^{null}$ homozygous photoreceptors, the basolateral and stalk membrane lengths were 8.08 ± 0.25 µm and 7.39 ± 0.39 µm and were 0.65× shorter and 1.40× longer than those of the wild-type photoreceptors, respectively. Adherence junctions (AJs) were located on the circumference of $Strat^{null}$ homozygous, Strat RNAi^{GD10605}-expressing, and $Rab10^{null}$ homozygous ommatidia, but in the central region of the wild-type ommatidia (Figure 2, A-J, and Supplemental Figure S2, A–J), likely because of the shorter basolateral and longer stalk membranes in the $Strat^{null}$ and $Rab10^{null}$ homozygous photoreceptors. These results indicate that the phenotypes of *Strat*-deficient photoreceptors were similar to those of $Rab10^{null}$ homozygous photoreceptors. However, unlike $Rab10^{null}$ homozygous photoreceptors, $Strat^{null}$ homozygous photoreceptors accumulated many vesicles in the cytoplasm and resembled Rab11RNAi^{pWIZ}-expressing photoreceptors (Figure 2, C, D, I, and J, and Supplemental Figure S2, C, D, I, and J). Strat RNAi^{GD10605}-expressing photoreceptors phenocopied the $Strat^{null}$ homozygous photoreceptors, but the same was not observed in $Strat^{WT}$ homozygous photoreceptors (Figure 2, E and F, and Supplemental Figure S2, E and F). These observations strongly indicate that both basolateral and rhabdomere transport are inhibited in *Strat*-deficient photoreceptors.

Strat is required for stable expression of Rab10 but not Rab11 in *Drosophila* photoreceptors

As *Strat*-deficient photoreceptors exhibited phenotypic characteristics of Rab10 and Rab11 deficiency, we next investigated the levels of Rab10 and Rab11 proteins in $Strat^{null}$ photoreceptors. In

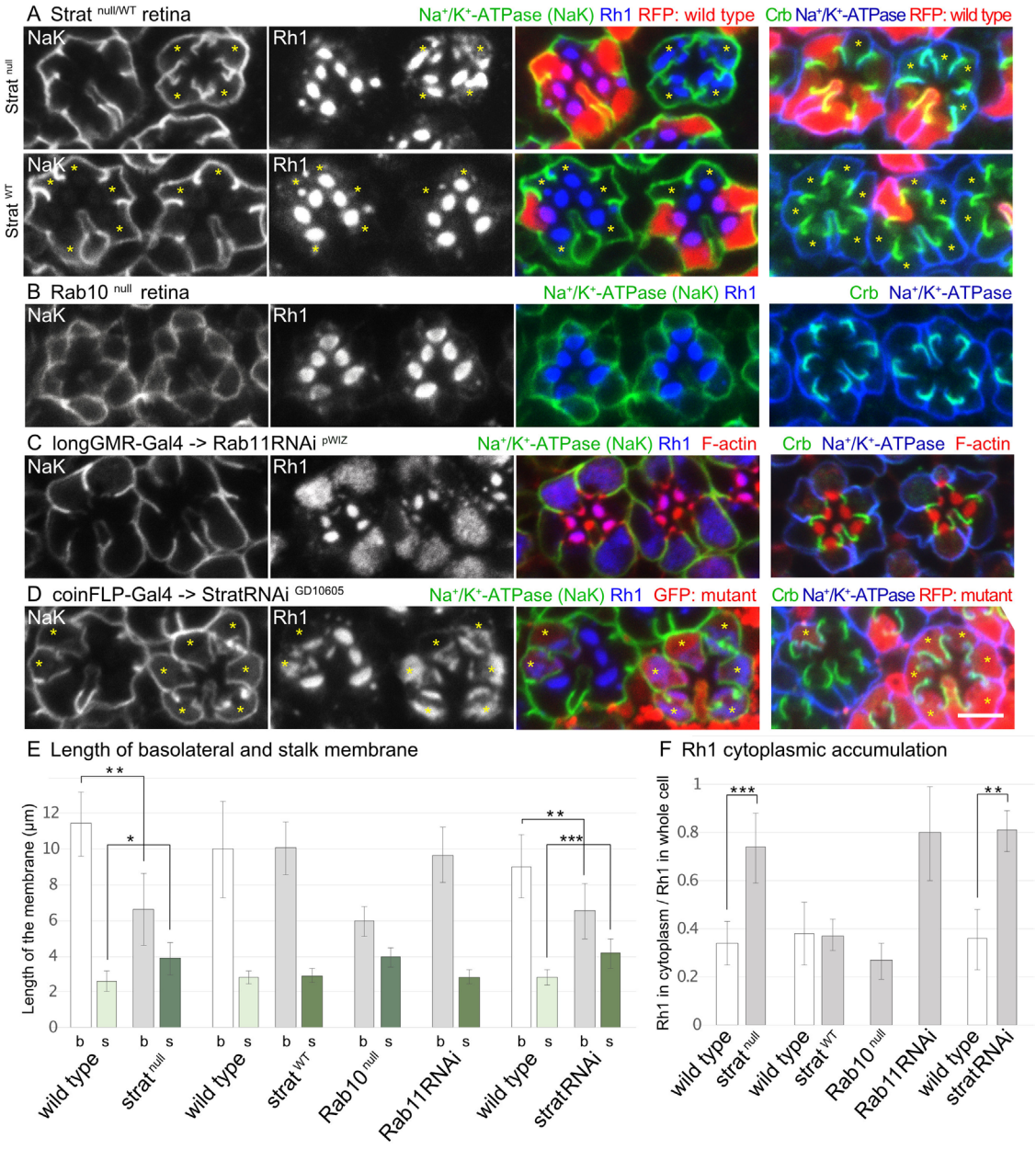

FIGURE 1: Impaired transport of both rhabdomeres and basolateral membrane in *Strat*-deficient photoreceptors. (A) Immunostaining of mosaic retinas from *Strat*^{null} (top panel) and *Strat*^{WT} (bottom panel) mosaic retina with anti-Na$^+$/K$^+$-ATPase-α (green) and anti-Rh1 (blue) antibodies (left) or anti-Crb (green) and Na$^+$/K$^+$-ATPase-α (blue) antibodies (right). RFP (red) shows the wild-type cells. Asterisks show *Strat*^{null} (top panel) and *Strat*^{WT} (bottom panel) cells. (B, C) Immunostaining of late pupal retinas from *Rab10*^{null} hemizygous flies (B) and *longGMR-Gal4/UAS-Rab11RNA*^{pWIZ} (C) with anti-Na$^+$/K$^+$-ATPase-α (green) and anti-Rh1 (blue) antibodies (left), or anti-Crb (green) and Na$^+$/K$^+$-ATPase-α (blue) antibodies (right). F-actin was stained with phalloidin (red). (D) Immunostaining of late pupal retinas from *coinFLP-Gal4/UAS-StratRNAi*^{GD10605} *UAS-GFP* flies with anti-Na$^+$/K$^+$-ATPase-α (green) and anti-Rh1 (blue) antibodies (left), or anti-Crb (green) and Na$^+$/K$^+$-ATPase-α (blue) antibodies (right). GFP (red) and asterisks indicate cells expressing StratRNAi^{GD10605}. (E) Lengths of the basolateral (white and gray) and stalk (light green and dark green) membranes of photoreceptors. The lengths of the membranes in the cross-sections of retinas stained with anti-Crb and Na$^+$/K$^+$-ATPase-α antibodies were measured using Fiji. A Crb-positive membrane was defined as a stalk membrane, and a Na$^+$/K$^+$-ATPase-α-positive but Crb-negative membrane was defined as a basolateral membrane. White and light green bars indicate the length of the basolateral and stalk membranes, respectively, of wild-type cells. Gray and dark green bars indicate the length of the basolateral and stalk membranes, respectively, of mutant cells in *Strat*^{null}, *Strat*^{WT}, *Rab10*^{null}, *longGMR-Gal4/UAS-Rab11RNAi*^{pWIZ}, and *coinFLP-Gal4/UAS-StratRNAi*^{GD10605}. (F) Plot of Rh1 cytoplasmic accumulation. In retinas stained with anti-Rh1 and Na$^+$/K$^+$-ATPase-α antibodies, the ratio of fluorescence intensity for Rh1 staining in the cytoplasm to that in whole cells was measured using Fiji. The details of the methodology for this measurement are described in *Materials and Methods*. White bars indicate wild-type cells, and gray bars indicate mutant cells in *Strat*^{null}, *Strat*^{WT}, *Rab10*^{null}, *longGMR-Gal4/UAS-Rab11RNAi*^{pWIZ}, and *coinFLP-Gal4/UAS-StratRNAi*^{GD10605}. Scale bar: 5 µm (A–D). Error bars indicate SD of three retinas. Significance according to two-tailed unpaired Student's *t* test: ***$p < 0.001$, **$p < 0.01$, and *$p < 0.02$.

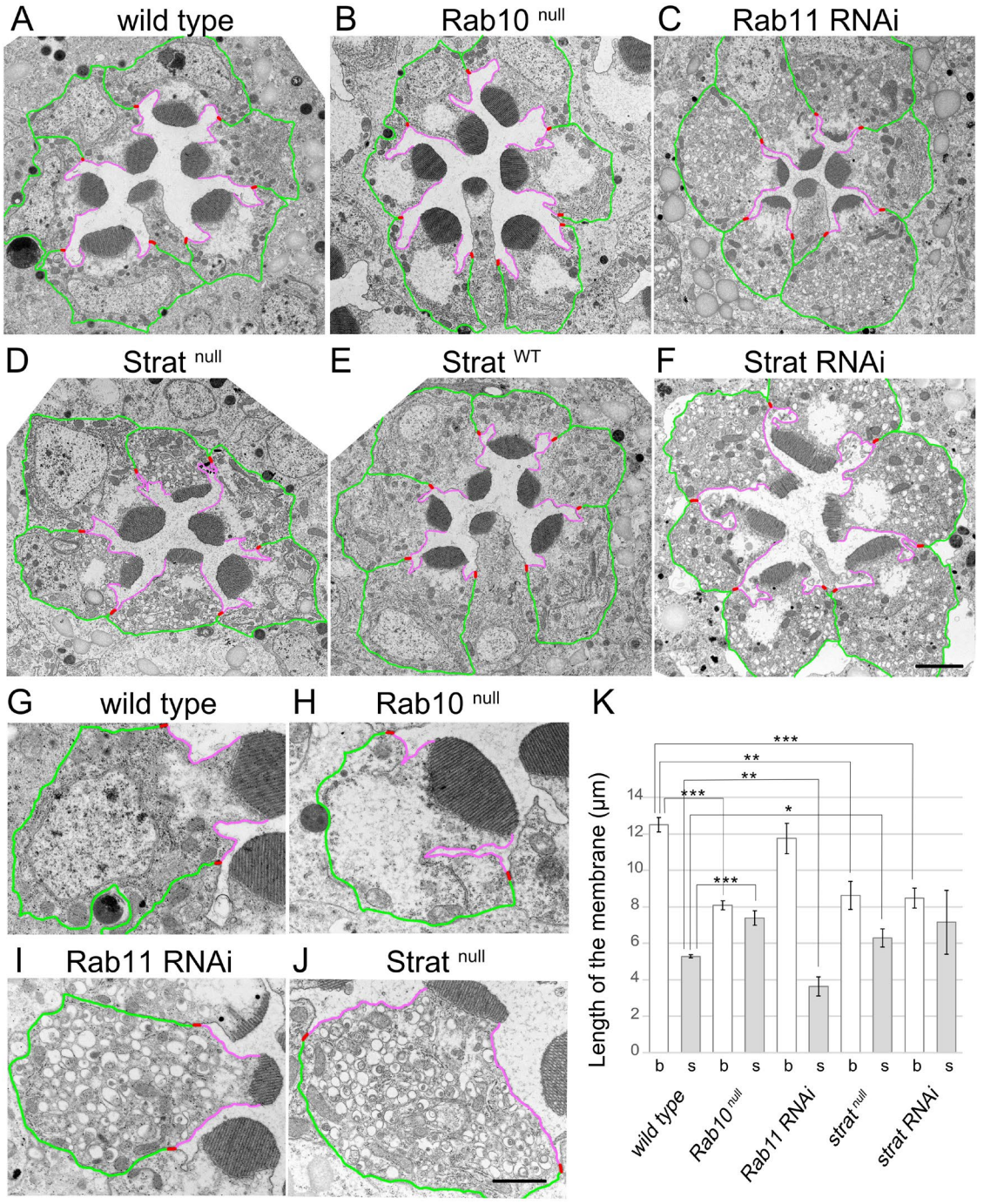

FIGURE 2: Ultrastructure of *Strat*-deficient photoreceptors. Green and pink lines indicate the basolateral and stalk membranes, respectively. AJs are indicated by the red boxes. (A–C) Electron micrographs of the wild-type fly, w^{1118} (A), $Rab10^{null}$ (B), and *longGMR-Gal4/UAS-Rab11RNAi*^{pWIZ} (C) ommatidia from late-pupal flies. (D, E) Electron micrographs of $Strat^{null}$ (D) and $Strat^{WT}$ (E) ommatidia obtained from a whole-eye homozygous clone of $Strat^{null}$ (D) and $Strat^{WT}$ (E) late pupal flies. (F) Electron micrographs of *StratRNAi*^{GD10605} expressing ommatidium obtained from *coinFLP-Gal4/UAS-StratRNAi*^{GD10605} late pupal flies. (G–I) Electron micrographs of wild-type flies and w^{1118} (G), $Rab10^{null}$ (H), and *longGMR-Gal4/UAS-Rab11RNAi*^{pWIZ} (I) photoreceptors from late pupal flies. (J) Electron micrographs of StratRNAi^{GD10605}-expressing photoreceptors obtained from *coinFLP-Gal4/UAS-StratRNAi*^{GD10605} in late-pupal flies. (K) Lengths of the basolateral (white) and stalk (gray) membranes of photoreceptors in wild-type, $Rab10^{null}$, *longGMR-Gal4/UAS-Rab11RNAi*^{pWIZ}, $Strat^{null}$, and *coinFLP-Gal4/UAS-StratRNAi*^{GD10605}. The lengths of the membranes in the retinas were measured using the Fiji software. Scale bars: 2 μm (A–F) and 1 μm (G–J). Error bars indicate SD of three retinas. Significance according to two-tailed unpaired Student's *t* test: ***$p < 0.001$, **$p < 0.01$, *$p < 0.05$.

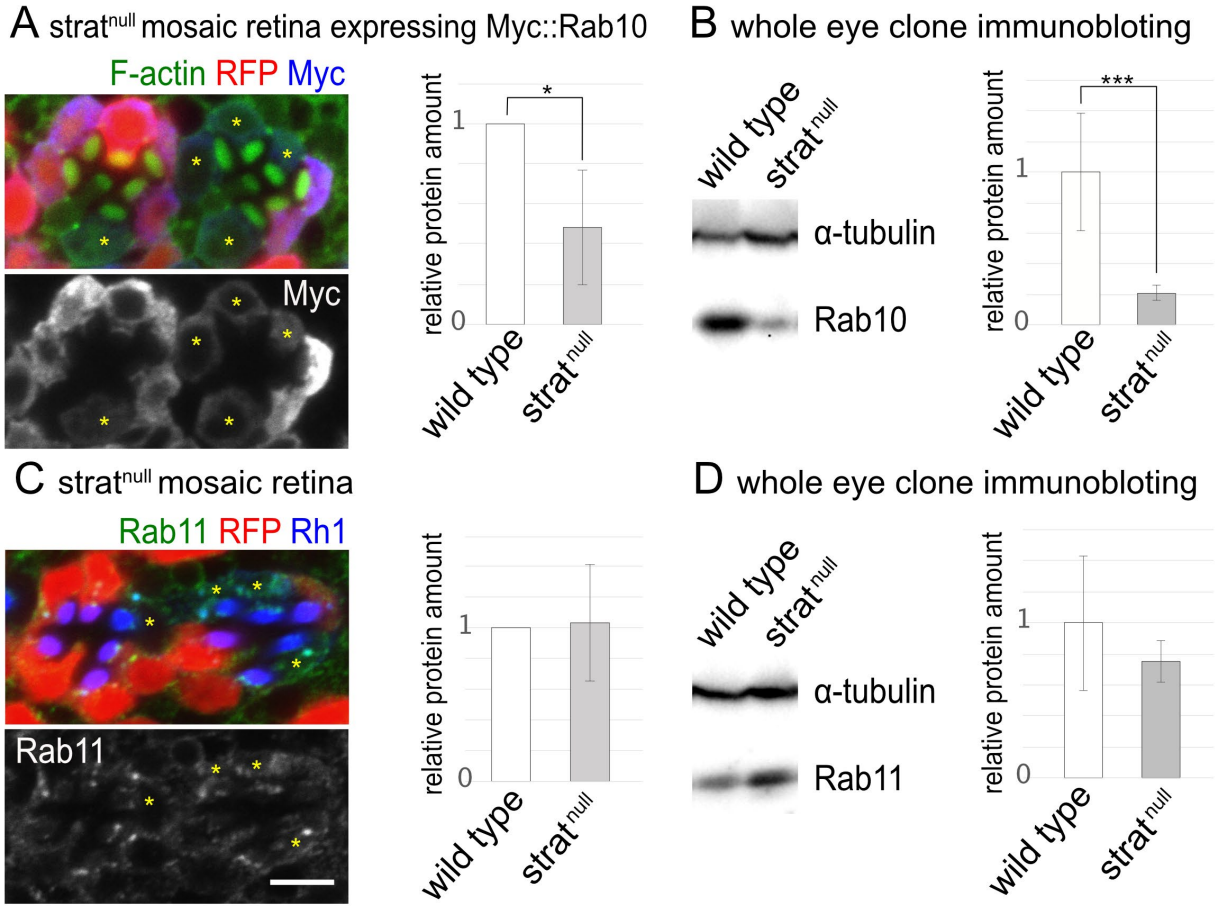

FIGURE 3: Rab10 but not Rab11 levels are reduced in *Strat*-deficient photoreceptors. (A) Immunostaining of *Strat*^{null} mosaic retinas expressing Myc::Rab10 with anti-Myc antibody (blue). F-actin was stained by phalloidin (green). RFP (red) shows the wild-type cells. Asterisks show *Strat*^{null} homozygous cells. Plot of the relative amounts of Myc::Rab10 in *Strat*^{null} photoreceptors as compared with those in wild-type photoreceptors. Error bars indicate SD of four retinas. Significance according to two-tailed unpaired Student's *t* test: $*p < 0.02$. (B) Immunoblotting of retinas from wild-type and a whole-eye homozygous clone of *Strat*^{null} flies with anti-α-tubulin and anti-Rab10 antibodies. Relative amounts of Rab10 in *Strat*^{null} retinas compared with those in wild-type retinas normalized by the amount of α-tubulin. Error bars indicate SD of 10 independent experiments. Significance according to two-tailed unpaired Student's *t* test: $***p < 0.001$. (C) Immunostaining of *Strat*^{null} mosaic retinas with anti-Rab11 (green) and anti-Rh1 (blue) antibodies. RFP (red) indicates the wild-type cells. Asterisks indicate the *Strat*^{null} homozygous cells. Relative amounts of Rab11 in *Strat*^{null} photoreceptors compared with those in wild-type photoreceptors. Error bars indicate SD of four retinas. Significance was determined using a two-tailed unpaired Student's *t* test. (D) Immunoblotting of retinas from the wild-type and a whole-eye homozygous clone of *Strat*^{null} flies with anti-α-tubulin and anti-Rab11 antibodies. Relative amounts of Rab11 in *Strat*^{null} retinas compared with wild-type retinas normalized by the amount of α-tubulin. Error bars indicate SD of 10 independent experiments. Significance was determined using a two-tailed unpaired Student's *t* test. Scale bar: 5 μm (A, C).

Strat^{null} mosaic retinas expressing myc::Rab10, the fluorescence signal of the anti-myc antibody was greatly reduced in *Strat*^{null} homozygous photoreceptors (52% reduction) as compared with that in the wild-type photoreceptors (Figure 3A). In line with this observation, immunoblotting of *Strat*^{null} whole-eye clones formed by the GMR-hid method (Stowers and Schwarz, 1999) and the wild-type eyes performed using anti-Rab10 antibody showed a 79% reduction in endogenous Rab10 levels in *Strat*^{null} whole-eye clones (Figure 3B and Supplemental Figure S3A). In contrast, endogenous Rab11 levels were not reduced in *Strat*^{null} homozygous photoreceptors or whole-eye clones both by immunostaining and immunoblotting (Figure 3, C and D, and Supplemental Figure S3B). These results indicate that Strat is required for stable expression of Rab10 but not Rab11 in *Drosophila* photoreceptors.

Rab35 is a novel Rab protein involved in rhabdomere transport

Strat^{null} homozygous photoreceptors showed Rh1 accumulation in the cytoplasm; however, *Strat* deficiency did not reduce Rab11 levels. We assumed that there is an unidentified Rab protein that is necessary for the post-Golgi transport of Rh1 and that its stable expression depends on Strat. Rab1, Rab3, Rab8, Rab10, Rab13, Rab15, and Rab35 were previously reported to bind to the mammalian ortholog Mss4 (Burton *et al.*, 1994; Strick *et al.*, 2002; Guruharsha *et al.*, 2011; Gulbranson *et al.*, 2017; Bellec *et al.*, 2018; Moissoglu *et al.*, 2020). Among these, Rab13 and Rab15 do not exist in the fly genome, and we have already shown that photoreceptors lacking Rab1 and Rab10 do not accumulate Rh1 in the cytoplasm (Satoh *et al.*, 1997; Nakamura *et al.*, 2020). Thus Rab3, Rab8, and Rab35 are strong candidates for Strat-dependent Rab proteins

that are essential for the post-Golgi transport of Rh1. We investigated whether the loss of Rab3, Rab8, or Rab35 affected the localization of Rh1 and Na^+/K^+-ATPase. The photoreceptors with a viable Rab3 null allele, *Rab3*^{rup}, over the deficient *Df*^{ED2076} showed normal localization of both Rh1 and Na^+/K^+-ATPase in the rhabdomere and basolateral membranes, respectively (Figure 4, A and F). As the hypomorphic allele *Rab8*^{1} (Giagtzoglou *et al.*, 2012) and Rab8 null allele *Rab8*^{del1} (produced in this work) are lethal, we generated mosaic retinas containing *Rab8*^{1} or *Rab8*^{del1} homozygous photoreceptors using the FLP/FRT method (Xu and Rubin, 1993). In both Rab8-deficient photoreceptors, Rh1 and Na^+/K^+-ATPase showed normal localization in the rhabdomere and basolateral membranes (Figure 4, B and F). In contrast, we observed severe cytoplasmic accumulation of Rh1 in Rab35RNAi^{JF02978}- and Rab35RNAi^{KK108660}-expressing photoreceptors (Figure 4, C, D, and F). In the electron micrograph, the cytoplasm of Rab35 knockdown photoreceptors was filled with vesicles and resembled those that accumulated in *Rab11*- or *Strat*-deficient photoreceptors (Figure 4, G and H). Na^+/K^+-ATPase was normally localized in the basolateral membrane of Rab35 RNAi^{JF02978}- and Rab35RNAi^{KK108660}-expressing photoreceptors (Figure 4, C and D). We also investigated Rab35^{null} hemizygous flies (Kohrs *et al.*, 2021) and found some accumulation of Rh1 in the cytoplasm (Figure 4E). The ratio of Rh1 in the Rab35^{null} hemizygous photoreceptor cytoplasm tended to be higher than that in the Rab35^{null}/+ heterozygous photoreceptor cytoplasm, but the difference was not statistically significant (Figure 4, E and F). The electron micrograph revealed the accumulation of some vesicles in the cytoplasm of Rab35^{null} hemizygous photoreceptors (Figure 4I), although the degree of accumulation was milder than that in Rab35RNAi^{JF02978}- and Rab35RNAi^{KK108660}-expressing photoreceptors. Our results indicated that neither Rab3 nor Rab8 but Rab35 is a candidate responsible for the post-Golgi transport of Rh1.

Strat is required for stable expression of Rab35

Next, we investigated Rab35 localization in fly photoreceptors. As three kinds of anti-Rab35 antibodies did not work for immunostaining of retinas (Zhang *et al.*, 2009), we generated transgenic flies with UAS-tagBFP2::FLAG::Rab35. In photoreceptors expressing tagBFP2::FLAG::Rab35, anti-FLAG antibody staining was observed exclusively in the rhabdomeres (Figure 5A). Rhabdomeres are tight bundles of microvilli that protrude from the apical plasma membrane. This result is consistent with many studies indicating Rab35 localization on the apical plasma membrane in mammalian cells (Klinkert *et al.*, 2016; Mrozowska and Fukuda, 2016).

We expressed tagBFP2::FLAG::Rab35 in *Strat*^{null} photoreceptors and found some anti-FLAG antibody staining in the cytoplasm but not in rhabdomeres (Figure 5B, left). The fluorescence intensity of anti-FLAG antibody staining in *Strat*^{null} photoreceptor rhabdomeres was 49% lower than that in wild-type photoreceptor rhabdomeres (Figure 5B, right). These results indicate that Rab35 is not functional without Strat. In agreement with the immunostaining results, immunoblotting of *Strat*^{null} whole-eye clones generated using the GMR-hid method (Stowers and Schwarz, 1999) and the wild-type eyes, performed using an anti-Rab35 antibody (Zhang *et al.*, 2009), showed a 55% reduction in endogenous Rab35 in *Strat*^{null} whole-eye clones (Figure 5C and Supplemental Figure S3C). Thus Strat is required for stable and functional Rab35 expression.

As both Rab11 and Rab35 are required for the post-Golgi Rh1 transport, we next investigated Rab11 localization in Rab35RNAi^{JF02978}-expressing photoreceptors. We found there is no Rab11 staining at the base of the rhabdomeres and Rab11 is colocalized with Rh1 in the cytoplasm (Figure 5D). This result indicates the possibility that Rab35 is required to tether Rh1 bearing post-Golgi vesicles to the base of the rhabdomeres.

DISCUSSION

In the present study, we found that Strat was required for both basolateral and rhabdomere transport through the stable expression of Rab10 and Rab35 (Figure 5E). We previously indicated that the reduction of Rab10 activity causes mislocalization of Na^+/K^+-ATPase to the stalk membrane, shrinkage of the basolateral membrane, and expansion of the stalk membrane, suggesting Rab10 is required for basolateral transport (Charron *et al.*, 2000). In our previous work, we failed to obtain *Rab10*^{null} flies; however, in this study, we successfully showed that *Rab10*^{null} photoreceptors indeed display these phenotypes. We found that in *Strat*-deficient photoreceptors, the amount of Rab10 protein was reduced, the basolateral membrane had shrunk, and Na^+/K^+-ATPase was mislocalized to the expanded stalk membrane. Rab10 reduction by the loss of Strat is consistent with the chaperon hypothesis and likely to be the reason of these phenotypes (Figure 5E).

We previously showed that Rab11 is localized at the *trans*-side of Golgi stacks and post-Golgi vesicles near the base of the rhabdomeres. Rab11, together with MyoV and dRip11, promotes the migration of post-Golgi vesicles toward the rhabdomere base (Satoh *et al.*, 2005; Li *et al.*, 2007). Here we found that in addition to basolateral transport, rhabdomere transport was inhibited in *Strat*-deficient photoreceptors. We failed to detect Rab11 reduction in *Strat*-deficient photoreceptors; however, we found that the protein levels of Rab35 were reduced. In the wild-type photoreceptors, Rab35 localizes exclusively at the rhabdomere membrane, which is the downstream of Rab11-mediated Rh1 transport. Moreover, Rab11 is lost at the base of the rhabdomeres and colocalized with Rh1 accumulated in cytoplasm of Rab35-deficient photoreceptors. Thus Rab35 is likely involved in tethering or fusion of Rh1-containing post-Golgi vesicles to the rhabdomere at the downstream of Rab11 (Figure 5E).

The function of Mss4 is under debate of whether it is a RabGEF or a chaperone for Rab proteins (Burton *et al.*, 1993; Moya *et al.*, 1993; Burton *et al.*, 1994; Miyazaki *et al.*, 1994; Nuoffer *et al.*, 1997; Coppola *et al.*, 2002; Strick *et al.*, 2002; Itzen *et al.*, 2006; Itzen *et al.*, 2007; Wu *et al.*, 2014; Gulbranson *et al.*, 2017). Recent studies support the role of Mss4 as a chaperone rather than RabGEF (Nuoffer *et al.*, 1997; Strick *et al.*, 2002; Itzen *et al.*, 2006; Itzen *et al.*, 2007; Wu *et al.*, 2014; Gulbranson *et al.*, 2017). In agreement with these studies, our data suggest that Strat functions as a chaperone for Rab10 and Rab35 in *Drosophila* photoreceptors, as Rab10 and Rab35 protein levels are greatly reduced in *Strat*-deficient retinas.

This is the first report to highlight the essential role of Rab35 in the post-Golgi transport of Rh1 to apical membrane rhabdomeres in *Drosophila* photoreceptors. Consistent with our results, several studies have indicated that Rab35 plays an important role in polarized transport to the apical membrane. Rab35 physically couples cytokinesis with the initiation of apico-basal polarity by tethering intracellular vesicles containing key apical determinants at the cleavage site (Klinkert *et al.*, 2016). Rab35 also regulates podocalyxin trafficking in two- and three-dimensional epithelial cell cultures, which are differentially activated by Rab35GEFs, DENND1A, and folliculin (Mrozowska and Fukuda, 2016; Kinoshita *et al.*, 2020). The I-Bar protein IRSp53 and the actin-capping protein EPS8 form a complex with Rab35 that is necessary for controlling the trafficking of apical determinants and maintaining the integrity of the luminal plasma membrane (Bisi *et al.*, 2020). Recent work has also indicated that CD13 establishes Rab35 at the apical membrane initiation site and

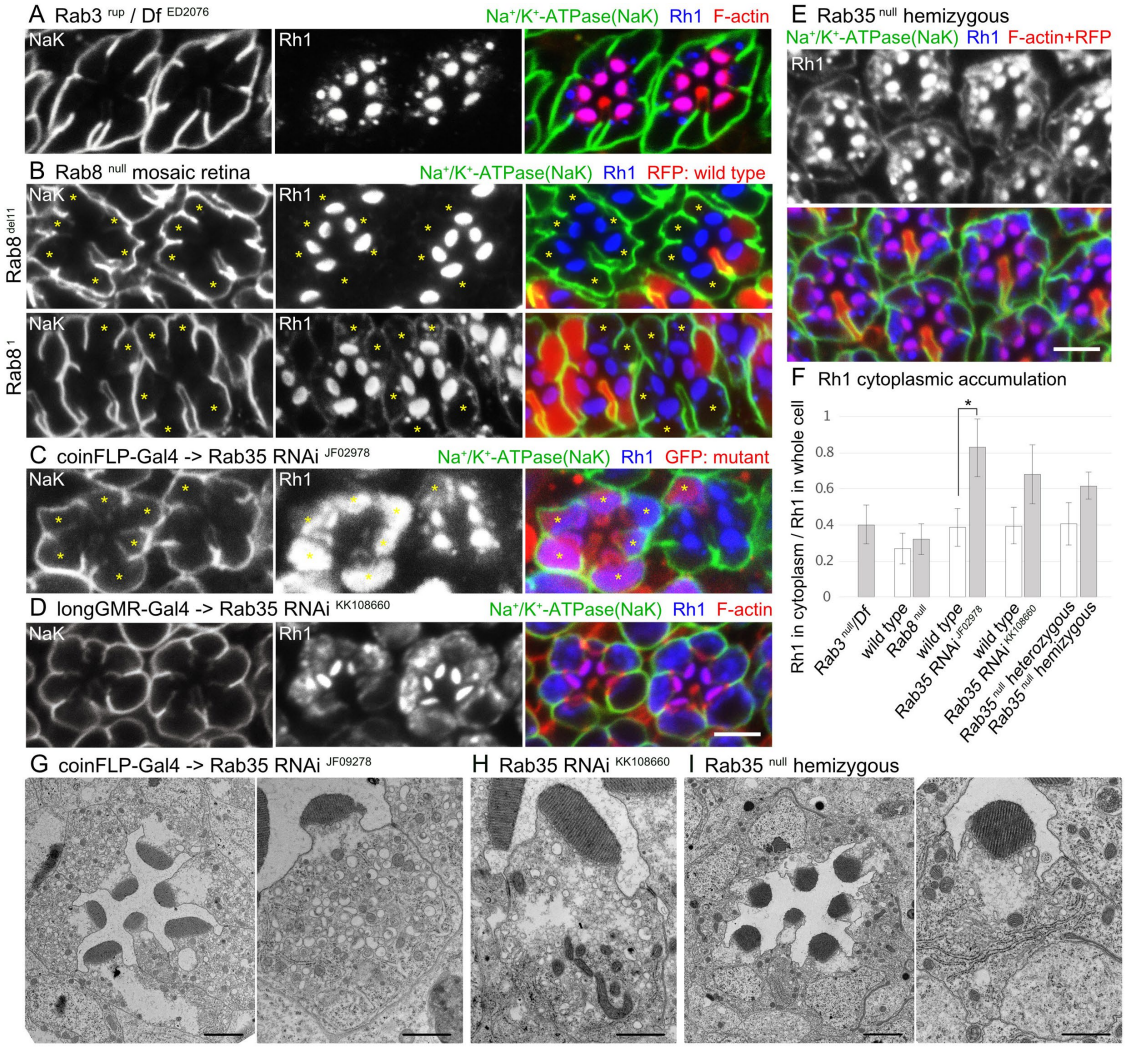

FIGURE 4: Impaired post-Golgi transport of rhabdomeres in Rab35-reduced photoreceptors. (A) Immunostaining of late pupal retinas from *Rab3*^{rup}/*Df*^{ED2076} flies with anti-Na$^+$/K$^+$-ATPase-α (green) and anti-Rh1 (blue) antibodies (left). F-actin was stained by phalloidin (red). (B) Immunostaining of mosaic retinas from *Rab8*^{del1l} (top panel) or *Rab8*^{1} (bottom panel) mosaic retina with anti-Na$^+$/K$^+$-ATPase-α (green) and anti-Rh1 (blue) antibodies (left). RFP (red) shows the wild-type cells. Asterisks show *Rab8*^{del11} *or Rab8*^{1} homozygous cells. (C) Immunostaining of late pupal retinas from *coinFLP-Gal4/UAS-Rab35RNAi*^{JF02978} flies with anti- Na$^+$/K$^+$-ATPase-α (green) and anti-Rh1 (blue) antibodies. GFP (red) and asterisks show cells with Rab35RNAi^{JF02978}. (D) Immunostaining of late pupal retinas from *longGMR-Gal4/UAS-Rab35RNAi*^{KK108660} flies with anti- Na$^+$/K$^+$-ATPase-α (green) and anti-Rh1 (blue) antibodies and phalloidin (red). (E) Immunostaining of late pupal retinas from *Rab35*^{null} hemizygous flies with anti- Na$^+$/K$^+$-ATPase-α (green) and anti-Rh1 (blue) antibodies and phalloidin (red). (F) The ratio of signal strength of Rh1 staining in the cytoplasm against that of the whole cells was plotted. White bars indicate the wild-type or Rab35 heterozygous cells, and the gray bars indicate mutant cells in *Rab3*^{rup}/*Df*^{ED2076}, *Rab8*^{null}, *coinFLP-Gal4/UAS-Rab35RNAi*^{JF02978}, *longGMR-Gal4/UAS-Rab35RNAi*^{KK108660}, and *Rab35*^{null} hemizygous flies. Error bars indicate SD of three retinas. Significance according to two-tailed unpaired Student's *t* test: *$p < 0.02$. (G) Electron micrographs of Rab35RNAi^{JF02978} ommatidium and the photoreceptor obtained from *coinFLP-Gal4/UAS-Rab35RNAi* ^{JF02978}. (H) Electron micrographs of Rab35RNAi^{KK108660} expressing photoreceptor by longGMR-Gal4. (I) Electron micrographs of *Rab35*^{null} hemizygous ommatidium and photoreceptors. Scale bar: 5 μm (A–E), 2 μm (G, I left panel) and 1 μm (G, I right panel and H).

is necessary for capturing vesicles containing apical determinates for apical membrane initiation (Wang *et al.*, 2021).

A recent report revealed an interesting interaction between Rab-11FIP1 and Rab35 and the critical role of Rab11FIP1 for Rab35 function in actin removal prior to cytokinesis. Interestingly, the *Drosophila* homolog of Rab11FIP1, dRip11, is essential for Rh1 transport in photoreceptors as well as cytokinesis and is localized to the intracellular bridge between daughter cells (Li *et al.*, 2007; Iannantuono and Emery, 2021). Future studies should explore the relationship between Rab11 and Rab35 in the final stage of Rh1 transport into the rhabdomeres.

MATERIALS AND METHODS

Request a protocol through *Bio-protocol*.

Drosophila stocks and genetic background

Drosophila were grown at 20–25°C on standard cornmeal–glucose–agar–yeast medium either in the laboratory with room light or in an

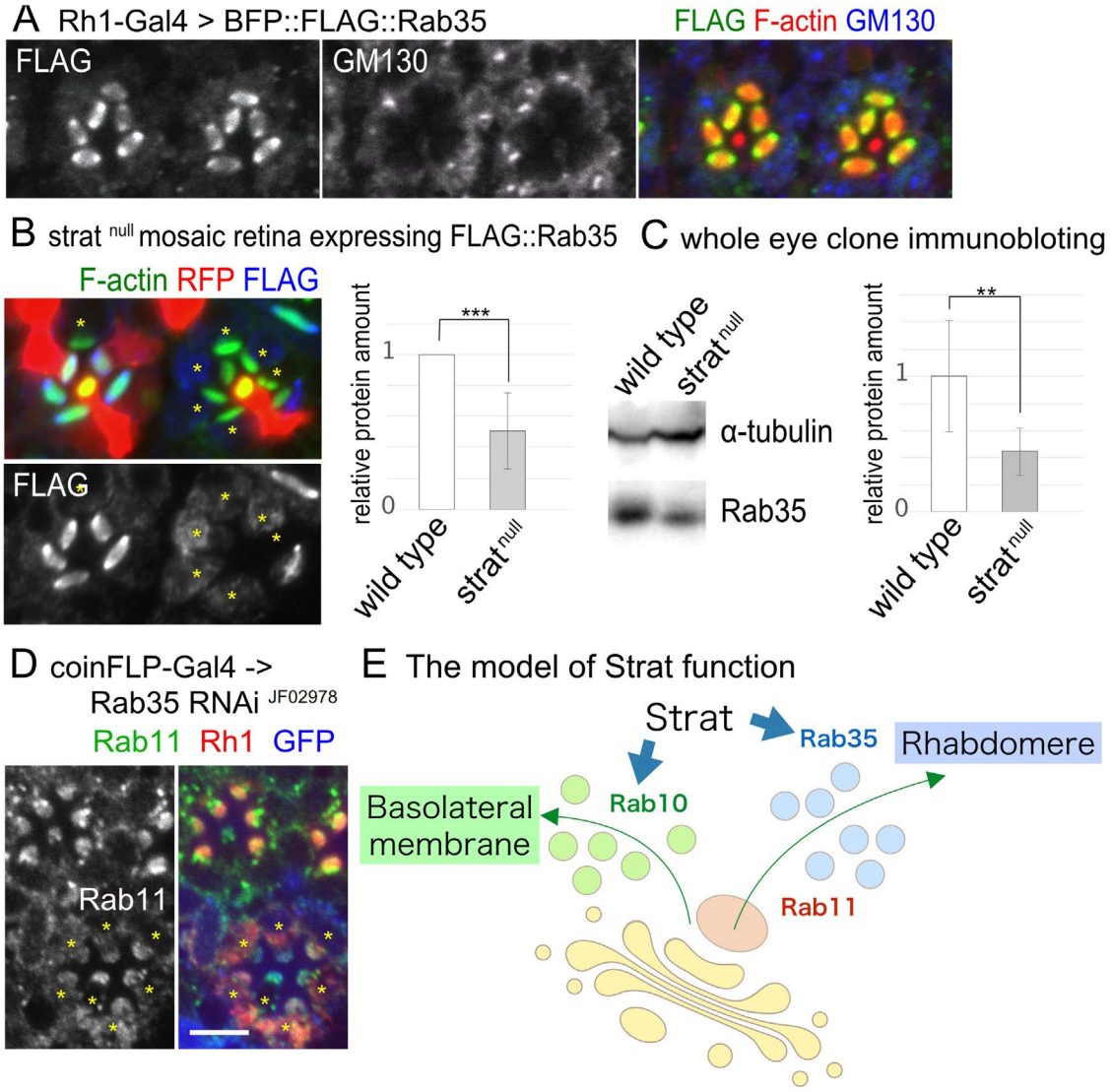

FIGURE 5: Rab35 levels are reduced in *Strat*-deficient photoreceptors. (A) Immunostaining of wild-type cells expressing tagBFP2::FLAG::Rab35 with anti-FLAG (green) and anti-GM130 (blue) antibodies. F-actin was stained by phalloidin (red). (B) Immunostaining of $Strat^{null}$ mosaic retinas expressing tagBFP2::FLAG::Rab35 by Rh1-Gal4 with anti-FLAG antibody (blue). F-actin was stained by phalloidin (green). RFP (red) shows the wild-type cells. Asterisks indicate the $Strat^{null}$ homozygous cells. Plot of the relative amounts of tagBFP2::FLAG::Rab35 in $Strat^{null}$ photoreceptors as compared with those in wild-type photoreceptors. Error bars indicate SD of five retinas. Significance according to two-tailed unpaired Student's *t* test: $***p < 0.001$. (C) Immunoblotting of retinas from wild-type and a whole-eye homozygous clone of $Strat^{null}$ with anti-α-tubulin and anti-Rab35 antibodies. Plot of the relative amounts of Rab35 in $Strat^{null}$ retinas as compared with those in the wild-type retinas normalized by the amount of α-tubulin. Error bars indicate SD of 10 independent experiments. Significance according to two-tailed unpaired Student's *t* test: $**p < 0.01$. (D) Immunostaining of late pupal retinas from *coinFLP-Gal4/UAS-Rab35RNAi*^{JF02978} flies with anti-Rab11 (green) and anti-Rh1 (red) antibodies. GFP (blue) and asterisks show cells with Rab35RNAi^{JF02978}. (E) The proposed model of functions of Strat and Rab proteins in polarized transport in *Drosophila* photoreceptors. Strat ensures the stable expression of Rab10 and Rab35, which regulate basolateral and rhabdomere transport, respectively. Rab11 is localized on *trans*-side of Golgi stacks and post-Golgi vesicles, and Rab35 is localized on the apical plasma membrane, rhabdomere. These localizations suggest that Rab35 works after Rab11 for Rh1 transport. Scale bar: 5 μm (A, B).

incubator without light. The following fly stocks were used: Rh1-Gal4 (Chihiro Hama, Kyoto Sangyo University, Japan), longGMR-Gal4 (Bloomington Drosophila Stock Center No. 8605, Bloomington, IN; indicated as BL8605 in the following stocks), coinFLP-Gal4 (BL58751), y w; GMR-hid FRT40A/CyO; ey-Gal4 UAS-FLP/TM6B flies (BL5250), UAS-Rab11RNAi^{pWIZ} (Satoh *et al.*, 2005), UAS-Strat RNAi^{GD10605} (Vienna Drosophila Resource Center No. 45715, Vienna, Austria; indicated as v45715 in the following stocks), Rab35RNAi^{JF02978} (BL28342), Rab35RNAi^{KK108660} (v101361), Rab-10^{null} /FM7, Rab35^{null} /FM7 (gifts from Hiesinger), and UAS-tagBFP2::FLAG::Rab35 (produced in the present study).

$Strat^{null}$ with RFP FRT40A/CyO and $Strat^{WT}$ with RFP FRT40A/CyO were kindly provided by Le Borgne (Bellec *et al.*, 2018) and RFP was removed using Cre recombinase (BL106201). Males of $Strat^{null}$ FRT40A/CyOGFP and $Strat^{WT}$ FRT40A/CyOGFP were crossed with y w eyFLP; RFP FRT40A/CyOGFP to generate mosaic eyes. *Rab8*^{1}

(BL26173) was combined with FRT80B. Males of *Rab8*^{1} FRT80B/TM6B were crossed with y w eyFLP; RFP FRT80B to generate mosaic eyes.

Construction of a *Rab8* null allele, *Rab8*^{del1}, and formation of *Rab8*^{del1} mosaic retinas

A null allele of *Rab8* was generated by FLP/FRT-based recombination between two P-element insertions, P{RS3}CB-5247-3 and P{RS3}CB-0752-3, located upstream and downstream of Rab8, respectively. Briefly, male flies carrying P{ry[+t7.2] = hsFLP}12 on X chromosome, P{RS3}CB-5247-3 and P{RS3}CB-0752-3 on the third chromosome were heat-treated at 37°C for 1 h daily for 3 d in larval stages. Isogenic lines balanced with TM6C were established and analyzed by PCR using genomic DNA as the template. The *Rab8* null allele, *Rab8*^{del1}, was identified by the presence of upstream of P{RS3}CB-5247-3 (amplified with primers Rab8-GF2 and 5′P-out) and downstream of P{RS3}CB-0752-3 (Rab8-GR1 and 3′P-out) but the absence of downstream of P{RS3}CB-5247-3 (Rab8-GR2 and 3′P-out) or upstream of P{R S3}CB-0752-3 (Rab8-GF1 and 5′P-out). To obtain *Rab8*^{del1} mosaic retinas, *Rab8*^{del1} was crossed with the original P-element insertion P{RS3}CB-5247-3, located on the proximal side of the Rab8 gene. Primer information; 5′P-out: 5′-CAAGCAAACGTGCACTGAAT-3′, 3′P-out: 5′-TCGCTGTCTCACTCAGAC

TCA-3′, Rab8-GF1: 5′-TTTTGTTGTCTGTGCCCGAG-3′, Rab8-GR1: 5′-GACCTATTT

TCTGCGGCTGG-3′, Rab8-GF2; 5′-GCGAAACAGTGCTAGTGGAG-3′, Rab8-GR2; 5′-CGGCCTAGGTCCCGTTTTAT-3′.

Transgenic flies for UAS-tagBFP2::FLAG::Rab35

The entire coding region of Rab35 was amplified from cDNA reverse-transcribed from total RNA extracted from the third instar larvae of the wild-type w^{1118} strain. The DNA fragment corresponding to A2 to the stop codon was integrated into a common P-element transformation vector pUAST together with N-terminal tagBFP2 connected with a FLAG tag linker encoding "TSGGDYKDDDDKGGGSGGGAAAGGRSGGGAPGGGGSGGGGSS" resulting in the plasmid vector pUAST-tBFP2-FLAG-Rab35. The plasmid was injected into embryos to generate transgenic lines.

Immunohistochemistry

Fixation and staining were performed as previously described, except for the fixative (Satoh and Ready, 2005). PLP (10 mM periodate, 75 mM lysine, 30 mM phosphate buffer, and 4% paraformaldehyde) was used as a fixative (Otsuka *et al.*, 2019). The primary antisera used were as follows: rabbit anti-Rh1 (1:1000) (Satoh *et al.*, 2005), mouse monoclonal anti-Na^{+}/K^{+}-ATPase alpha subunit (1:500 ascites; Developmental Studies Hybridoma Bank [DSHB], Iowa City, IA), rat anti-Crb (1:300) (Ulrich Tepass, University of Toronto, Toronto, Ontario, Canada), rat anti-Rab11 (1:250) (Otsuka *et al.*, 2019), mouse monoclonal anti-myc (1:12; DSHB), rabbit anti-myc (1:300) (Medical and Biological Laboratories Co., Nagoya, Japan; No. 562), and mouse anti-FLAG M2 (1:1000) (Sigma-Aldrich Japan, Tokyo, Japan). The secondary antibodies were anti-mouse, anti-rabbit, and/or anti-rat antibodies labeled with Alexa Fluor 488 and 647 (1:300) (Life Technologies, Carlsbad, CA) or Cy2 (1:300) (GE Healthcare Life Sciences, Pittsburgh, PA). F-actin was stained with phalloidin conjugated with Alexa Fluor 568 (Life Technologies, Carlsbad, CA). Sample images were recorded using a Model FV1000 confocal microscope (60× 1.42 NA objective lens; Olympus, Tokyo, Japan). To minimize bleed-through, each signal in the double- or triple-stained samples was sequentially imaged. Images were processed following the Guidelines for Proper Digital Image Handling using ImageJ and affinity photos. To quantify the intensity of Rh1 staining in the photoreceptor cytoplasm, we used more than three mosaic retinas with more than eight wild-type and eight mutant photoreceptors in each retina. The area of the cytoplasm or whole cells and their staining intensities were measured using Fiji (Schindelin *et al.*, 2012). Na^{+}/K^{+}-ATPase-α and Rh1 staining were used to define the outline of the cell and rhabdomere. Rhabdomeres were defined as Rh1-positive oval structures protruding from the photoreceptors to the center of the ommatidium. The area of the cells, except for the rhabdomere, was regarded as the cytoplasm. The integrated densities of Rh1 staining in cytoplasm and whole cells were measured. The ratio of the density of cytoplasm to that of whole cell was calculated for each cell. The sectional lengths of the stalk (defined as the membrane stained by anti-Crb antibody and used as the sum of both sides of the rhabdomere) and basolateral membrane (defined as the membrane stained with anti-Na^{+}/K^{+}-ATPase-α antibody but not by anti-Crb antibody) were measured using Fiji. More than five photoreceptors in three flies for more than three independent samples for each genotype were used for these measurements.

Electron microscopy

Electron microscopy was performed as previously described (Satoh *et al.*, 1997). The samples were observed under a JEM1400 electron microscope (JEOL, Tokyo, Japan), and montages were prepared using a charge-coupled device camera system (JEOL). The phenotypes were investigated using a section at the depth at which a couple of photoreceptor nuclei within the ommatidia were observed.

Immunoblotting

For quantitative isolation of the retina, we used freeze-dried flies stored in acetone (Fujita *et al.*, 1987; Nakamura *et al.*, 2020). *W; GMR-hid 40A/ Strat*^{null} *FRT40A; ey-Gal4 UAS-FLP/+* flies and *w; GMR-hid FRT40A/+; ey-Gal4 UAS-FLP/+* flies at 0–7 d were collected and frozen in liquid nitrogen. The heads were collected using two sieves with different mesh sizes. The heads were then immersed in acetone, cooled to −80°C, and maintained for >1 wk. The acetone was replaced once or twice during this time to remove water. The retinas were dissected with forceps, and the proteins were extracted in SDS sample buffer (0.05 M Tris, 10% vol/vol glycerol, 5% vol/vol β-mercaptoethanol, and 2.3% wt/vol SDS) in phosphate buffer solution at 80°C for 2 min. Ten independent samples, each containing 40 eyes in 40 µl SDS sample buffer, were prepared for both the wild-type and a whole-eye homozygous clone of *Strat*^{null}.

Immunoblotting was performed as previously described (Satoh *et al.*, 1997). The blotted membranes were cut, the upper halves were used to detect α-tubulin as loading controls, and the lower halves were used to detect Rab proteins. Mouse anti-α-tubulin (1:200 supernatant) (DSHB), guinea pig anti-Rab10 (1:2500) (Nakamura *et al.*, 2020), rat anti-Rab11 (1:2500) (Otsuka *et al.*, 2019), and rabbit anti-Rab35 (1:1000) (Zhang *et al.*, 2009) were used as the primary antibodies. HRP–conjugated anti-mouse, anti-rabbit, anti-rat, and anti-guinea pig IgG antibodies (1:20 000; Life Technologies) were used as secondary antibodies. The signals were visualized by enhanced chemiluminescence (Clarity Western ECL Substrate; Bio-Rad, Hercules, CA) and imaged using ChemiDoc XRS+ (Bio-Rad). The intensities of the 60 bands were measured using Fiji software, the intensity of the α-tubulin band was used to standardize the loading amount for each lane, and the amounts of Rab proteins between the wild-type and *Strat*^{null} mutant retinas were compared.

ACKNOWLEDGMENTS

We thank U. Tepass, P. Hiesinger, M.P. Scott, and R. Le Borgne for kindly providing fly stocks and reagents. We also thank the Bloomington Drosophila Stock Center (Indiana University, IN) and the Vienna Drosophila Resource Center (Viena BioCenter, Vienna, Austria) for their fly stocks. We thank Editage (www.editage.jp) for English language editing. This work was supported by Precursory Research for Embryonic Science and Technology (Grant No. 25-J-J4215), Core Research for Organelle Diseases in Hiroshima University, Japan Society for the Promotion of Science, Takeda Science Foundation, Ohsumi Frontier Science Foundation, KAKENHI (Grants No. 15K07050, No. 19K06663, and No. 22H02617) to A.S., and KAKENHI (Grant No. 19K06566) to T.S.

REFERENCES

Bellec K, Gicquel I, Le Borgne R (2018). Stratum recruits Rab8 at Golgi exit sites to regulate the basolateral sorting of Notch and Sanpodo. Development 145, 163469.

Bellec K, Pinot M, Gicquel I, Le Borgne R (2020). The Clathrin adaptor AP-1 and Stratum act in parallel pathways to control Notch activation in *Drosophila* sensory organ precursors cells. Development, 148, 191437.

Bisi S, Marchesi S, Rizvi A, Carra D, Beznoussenko GV, Ferrara I, Deflorian G, Mironov A, Bertalot G, Pisati F, *et al.* (2020). IRSp53 controls plasma membrane shape and polarized transport at the nascent lumen in epithelial tubules. Nat Commun 11, 3516.

Burton J, Roberts D, Montaldi M, Novick P, De Camilli P (1993). A mammalian guanine-nucleotide-releasing protein enhances function of yeast secretory protein Sec4. Nature 361, 464–467.

Burton JL, Burns ME, Gatti E, Augustine GJ, De Camilli P (1994). Specific interactions of Mss4 with members of the Rab GTPase subfamily. EMBO J 13, 5547–5558.

Charron AJ, Bacallao RL, Wandinger-Ness A (2000). ADPKD: a human disease altering Golgi function and basolateral exocytosis in renal epithelia. Traffic 1, 675–686.

Coppola T, Perret-Menoud V, Gattesco S, Magnin S, Pombo I, Blank U, Regazzi R (2002). The death domain of Rab3 guanine nucleotide exchange protein in GDP/GTP exchange activity in living cells. Biochem J 362, 273–279.

Devergne O, Sun GH, Schüpbach T (2017). Stratum, a homolog of the human GEF Mss4, partnered with Rab8, controls the basal restriction of basement membrane proteins in epithelial cells. Cell Rep 18, 1831–1839.

Fujita SC, Inoue H, Yoshioka T, Hotta Y (1987). Quantitative tissue isolation from Drosophila freeze-dried in acetone. Biochem J 243, 97–104.

Giagtzoglou N, Yamamoto S, Zitserman D, Graves HK, Schulze KL, Wang H, Klein H, Roegiers F, Bellen HJ (2012). dEHBP1 controls exocytosis and recycling of Delta during asymmetric divisions. J Cell Biol 196, 65–83.

Gulbranson DR, Davis EM, Demmitt BA, Ouyang Y, Ye Y, Yu H, Shen J (2017). RABIF/MSS4 is a Rab-stabilizing holdase chaperone required for GLUT4 exocytosis. Proc Natl Acad Sci USA 114, E8224–E8233.

Guruharsha KG, Rual JF, Zhai B, Mintseris J, Vaidya P, Vaidya N, Beekman C, Wong C, Rhee DY, Cenaj O, *et al.* (2011). A protein complex network of Drosophila melanogaster. Cell 147, 690–703.

Iannantuono NVG, Emery G (2021). Rab11FIP1 maintains Rab35 at the intercellular bridge to promote actin removal and abscission. J Cell Sci 134, 244384.

Li BX, Satoh AK, Ready DF (2007). Myosin V, Rab11, and dRip11 direct apical secretion and cellular morphogenesis in developing Drosophila photoreceptors. J Cell Biol 177, 659–669.

Itzen A, Pylypenko O, Goody RS, Alexandrov K, Rak A (2006). Nucleotide exchange via local protein unfolding–structure of Rab8 in complex with MSS4. EMBO J 25, 1445–1455.

Itzen A, Rak A, Goody RS (2007). Sec2 is a highly efficient exchange factor for the Rab protein Sec4. J Mol Biol 365, 1359–1367.

Kinoshita R, Homma Y, Fukuda M (2020). Rab35-GEFs, DENND1A and folliculin differentially regulate podocalyxin trafficking in two- and three-dimensional epithelial cell cultures. J Biol Chem 295, 3652–3663.

Klinkert K, Rocancourt M, Houdusse A, Echard A (2016). Rab35 GTPase couples cell division with initiation of epithelial apico-basal polarity and lumen opening. Nat Commun 7, 11166.

Kohrs FE, Daumann IM, Pavlovic B, Jin EJ, Kiral FR, Lin SC, Port F, Wolfenberg H, Mathejczyk TF, Linneweber GA, *et al.* (2021). Systematic functional analysis of rab GTPases reveals limits of neuronal robustness to environmental challenges in flies. eLife 10, 59594.

Laffafian A, Tepass U (2019). Identification of genes required for apical protein trafficking in *Drosophila* photoreceptor cells. G3 (Bethesda) 9, 4007–4017.

Miyazaki A, Sasaki T, Araki K, Ueno N, Imazumi K, Nagano F, Takahashi K, Takai Y (1994). Comparison of kinetic properties between MSS4 and Rab3A GRF GDP/GTP exchange proteins. FEBS Lett 350, 333–336.

Moissoglu K, Stueland M, Gasparski AN, Wang T, Jenkins LM, Hastings ML, Mili S (2020). RNA localization and co-translational interactions control RAB13 GTPase function and cell migration. EMBO J 39, e104958.

Moya M, Roberts D, Novick P (1993). DSS4-1 is a dominant suppressor of sec4-8 that encodes a nucleotide exchange protein that aids Sec4p function. Nature 361, 460–463.

Mrozowska PS, Fukuda M (2016). Regulation of podocalyxin trafficking by Rab small GTPases in 2D and 3D epithelial cell cultures. J Cell Biol 213, 355–369.

Nakamura Y, Ochi Y, Satoh T, Satoh AK (2020). Rab10, Crag and Ehbp1 regulate the basolateral transport of Na^+ K^+ ATPase in *Drosophila* photoreceptors. J Cell Sci 133, 238790.

Nuoffer C, Wu SK, Dascher C, Balch WE (1997). Mss4 does not function as an exchange factor for Rab in endoplasmic reticulum to Golgi transport. Mol Biol Cell 8, 1305–1316.

Otsuka Y, Satoh T, Nakayama N, Inaba R, Yamashita H, Satoh AK (2019). Parcas is the predominant Rab11-GEF for rhodopsin transport in *Drosophila* photoreceptors. J Cell Sci 132, 231431.

Pfeffer SR (2013). Rab GTPase regulation of membrane identity. Curr Opin Cell Biol 25, 414–419.

Román-Fernández A, Bryant DM (2016). Complex polarity: building multicellular tissues through apical membrane traffic. Traffic 17, 1244–1261.

Satoh A, Tokunaga F, Kawamura S, Ozaki K (1997). In situ inhibition of vesicle transport and protein processing in the dominant negative Rab1 mutant of Drosophila. J Cell Sci 110 (Pt 23), 2943–2953.

Satoh AK, O'Tousa JE, Ozaki K, Ready DF (2005). Rab11 mediates post-Golgi trafficking of rhodopsin to the photosensitive apical membrane of Drosophila photoreceptors. Development 132, 1487–1497.

Satoh AK, Ready DF (2005). Arrestin1 mediates light-dependent rhodopsin endocytosis and cell survival. Curr Biol 15, 1722–1733.

Schindelin J, Arganda-Carreras I, Frise E, Kaynig V, Longair M, Pietzsch T, Preibisch S, Rueden C, Saalfeld S, Schmid B, *et al.* (2012). Fiji: an open-source platform for biological-image analysis. Nat Methods 9, 676–682.

Schopf K, Huber A (2017). Membrane protein trafficking in Drosophila photoreceptor cells. Eur J Cell Biol 96, 391–401.

Stenmark H (2009). Rab GTPases as coordinators of vesicle traffic. Nat Rev Mol Cell Biol 10, 513–525.

Stowers RS, Schwarz TL (1999). A genetic method for generating Drosophila eyes composed exclusively of mitotic clones of a single genotype. Genetics 152, 1631–1639.

Strick DJ, Francescutti DM, Zhao Y, Elferink LA (2002). Mammalian suppressor of Sec4 modulates the inhibitory effect of Rab15 during early endocytosis. J Biol Chem 277, 32722–32729.

Tepass U, Harris KP (2007). Adherens junctions in Drosophila retinal morphogenesis. Trends Cell Biol 17, 26–35.

Wang LT, Rajah A, Brown CM, McCaffrey L (2021). CD13 orients the apical-basal polarity axis necessary for lumen formation. Nat Commun 12, 4697.

Wu L, Xu D, Zhou L, Xie B, Yu L, Yang H, Huang L, Ye J, Deng H, Yuan YA, *et al.* (2014). Rab8a-AS160-MSS4 regulatory circuit controls lipid droplet fusion and growth. Dev Cell 30, 378–393.

Xiong B, Bellen HJ (2013). Rhodopsin homeostasis and retinal degeneration: lessons from the fly. Trends Neurosci 36, 652–660.

Xu T, Rubin GM (1993). Analysis of genetic mosaics in developing and adult Drosophila tissues. Development 117, 1223–1237.

Zhang J, Fonovic M, Suyama K, Bogyo M, Scott MP (2009). Rab35 controls actin bundling by recruiting fascin as an effector protein. Science 325, 1250–1254.